Enhanced persistent photoconductivity in δ-doped $LaAlO_3/SrTiO_3$ heterostructures

A. Rastogi,[1] J. J. Pulikkotil,[2] and R. C. Budhani[1,2,*]

[1]*Condensed Matter Low Dimensional Systems Laboratory, Department of Physics, Indian Institute of Technology, Kanpur 208016, India*
[2]*Division of Quantum Phenomena and Applications, CSIR–National Physical Laboratory, Dr. K. S. Krishnan Marg, New Delhi 110012, India*

(Received 23 October 2013; revised manuscript received 15 March 2014; published 31 March 2014)

We report the effect of δ doping at the $LaAlO_3/SrTiO_3$ interface with $LaMnO_3$ monolayers on the photoconducting (PC) state. The PC is realized by exposing the samples to broadband optical radiation of a quartz lamp and 325 and 441 nm lines of a He-Cd laser. Along with the significant modification in electrical transport which drives the pure $LaAlO_3/SrTiO_3$ interface from metal-to-insulator with increasing $LaMnO_3$ sub-monolayer thickness, we also observe an enhancement in the photoresponse and relaxation time constant. A possible scenario for the PC based on defect clusters, random potential fluctuations, and large lattice relaxation models, along with the role of structural phase transition in $SrTiO_3$, is discussed. For pure $LaAlO_3/SrTiO_3$, the photoconductivity appears to originate from interband transitions between Ti-derived 3d bands which are e_g in character and O 2p–Ti t_{2g} hybridized bands. The band structure changes significantly when fractional layers of $LaMnO_3$ are introduced. Here the Mn e_g bands ($\approx$1.5 eV above the Fermi energy) within the photoconducting gap lead to a reduction in the photoexcitation energy and a gain in overall photoconductivity.

DOI: 10.1103/PhysRevB.89.125127 PACS number(s): 73.40.−c, 73.50.Pz, 68.55.Ln, 71.30.+h

I. INTRODUCTION

The origin of the two-dimensional electron gas (2DEG) at the interface of artificially tailored oxide heterostructures [1–5] is attributed to both intrinsic and extrinsic factors. While the former are accounted for in the polar catastrophe model [6,7], extrinsic factors are associated with defects, such as oxygen vacancies [8–10] and intersite cation mixing [11,12] that are introduced in the system during film growth [13,14]. The latter argument is substantiated by the observation of a clear dependence of the interface conductivity on pressure during the film growth [6,14]. Furthermore, the observation of persistent photoconductivity (PPC) with large relaxation time also points to the role of defect-induced states in these oxide heterostructures [15–17]. However, there also exists conclusive evidence that defects in the form of O vacancies in the $SrTiO_3$ substrate are not the only responsible factor that leads to 2DEG at the interface. Had this been the case, then irrespective of the nature of the films, a 2DEG would have been observed for most of the perovskite oxides deposited on $SrTiO_3$, including for $LaCrO_3$ and $LaMnO_3$. Beyond this, we note that doping induces electronic phase transitions and metallicity in both $LaCrO_3$ and $LaMnO_3$ [18–20]. On the other hand, transport measurements find that the $LaCrO_3$ and $LaMnO_3$ films deposited on TiO_2-terminated $SrTiO_3$ substrate results in no 2DEG at the interface, irrespective of the film thickness and deposition conditions [21,22].

In general, a 2DEG state is observed at the interface of a nonpolar (TiO_2-terminated $SrTiO_3$) and a polar material (such as $LaAlO_3$) motif. Under these circumstances, the in-built electric field at the interface causes bending of conduction and valence band edges of $SrTiO_3$, leading to a triangular potential well which is filled by electrons transferred from the $LaAlO_3$ overlayers [23–28]. Although this model explains many of the experimental observations, it fails to account for the observed charge carrier density that has its dependence on the thickness of the deposited $LaAlO_3$ film [4,5]. Beyond this, the model also has little support from the photoemission spectroscopy studies [29–32].

A fundamental understanding of the underlying mechanism for the formation of the 2DEG therefore requires use of perturbative techniques, which will lead to injection of additional charge carriers at the interface and selective and controlled modification of the interface chemistry. While the former is realized by electrostatic gating and photoexcitation [4,15,17], the latter can be achieved by δ doping at the interface, a concept commonly used in III-V compound semiconductor quantum wells [33].

The effect of electrostatic gating of the $LaAlO_3/SrTiO_3$ interface has been studied extensively. The gate field either draws charges towards the interface from the overlayers or pushes charge towards it resulting in a gate-controlled metal-insulator phase transition [4,34]. It has also been shown earlier that the electronic transport in oxide heterostructures can be altered significantly on exposure to electromagnetic radiation of optical frequency making these potential candidates in optoelectronic applications [15–17]. For the conducting interface of $LaTiO_3/SrTiO_3$ and $LaAlO_3/SrTiO_3$, the PPC is seen in the spectral range of 300–400 nm. It is also noticed that the magnitude and relaxation dynamics of the photoconducting state depends on the growth temperature of $LaTiO_3$ and $LaAlO_3$, but is independent of the number of the film overlayers, since the response is only energetically close to the band gap of $SrTiO_3$. It has been previously shown that $SrTiO_3$ (single crystal and thin films) displays a wide range of properties such as ferroelectric [35,36] ones and persistent photoconductivity [37]. Therefore, it is quite evident that the $SrTiO_3$ substrate plays a crucial role in determining the electronic and optical properties in these heterostructures. The PPC seen in oxide interfaces is quite similar to that reported in the III-V semiconductor heterostructures [38,39]. In analogy with the latter systems, the slow decay of the photocurrent in oxides can be associated with the defect-induced states in the $SrTiO_3$ substrate. The recovery process in these oxide heterostructures has two distinct activation energies

*rcb@nplindia.org

 ©2014 American Physical Society

below and above ≈100 K. This appears to be related to the quantum paraelectric nature of $SrTiO_3$ which results in precipitous growth of its dielectric function below 100 K, and increase in the Bohr radius of Ti $3d^1$ electrons near oxygen vacancy sites.

We have observed a systematic metal-to-insulator transition in the $LaAlO_3/SrTiO_3$ system by controlled δ doping at the interface with $LaMnO_3$ monolayers [40]. Our present experiment rules out the possibility of interfacial intermixing as the cause of metallic conduction in the $LaAlO_3/SrTiO_3$ system, because such a reaction of La/Sr at the interface would lead to formation of $La_{1-x}Sr_xTiO_3$ which should be conducting based on the simple valence argument. Our experiment also rules out the reduction of $SrTiO_3$ as the cause of 2DEG, as reduction would take place even in the case of δ-$LaMnO_3$ monolayer deposition, resulting in interfacial conductivity irrespective of the Mn concentration at the interface. While the present experiment validates the polarization catastrophe argument for the 2DEG formation, it remains to be seen what would happen to photoconductivity when transfer of electrons from $LaAlO_3$ overlayers is inhibited by the δ-$LaMnO_3$ monolayer.

Here we present the results of photoconductivity measurements on the δ-doped $LaAlO_3/SrTiO_3$ heterostructures, and compared them with the photoresponse of the undoped $LaAlO_3/SrTiO_3$ system. It has been shown previously that $LaMnO_3$ films on $SrTiO_3$ remain nonconducting irrespective of their thickness [22]. Therefore, a controlled deposition of Mn ions at the $LaAlO_3/SrTiO_3$ interface is expected to provide a method to control the electronic phases and phase transition. In accordance, we find that the resistivity of the δ-doped $LaAlO_3/SrTiO_3$ increases nontrivially as the δ-$LaMnO_3$ monolayer at the interface is thickened. Beyond this, the results of photo-conductivity measurements reported here also include the following: (i) a larger photoresponse with increasing δ-doped $LaMnO_3$ interfacial layer thickness and (ii) persistent photoconductivity following a stretched exponential behavior with its decay constant increasing in proportion with the $LaMnO_3$ monolayer thickness. Explanation of these results is sought in terms of a few well-established models and also partly from the band structure calculations.

II. EXPERIMENTAL DETAILS

The samples were grown by pulsed-laser deposition at 800 °C and the thickness of $LaAlO_3$ deposited on TiO_2-terminated (001) $SrTiO_3$ was kept at 20 unit cells (uc). The deposition procedure, conditions, and growth parameters are described in our earlier reports [16,17,40]. The δ doping of the interface has been achieved by controlled growth (≃0.012–0.015 nm/s) of a $LaMnO_3$ sub-monolayer prior to commencing deposition of $LaAlO_3$ film. In its bulk form, $LaMnO_3$ is a strongly correlated antiferromagnetic insulator. A schematic of the interfacial δ doping with $LaMnO_3$ is shown in the inset of Fig. 1. To perform the transport measurements, Ag/Cr electrodes were deposited on the films (drain and source) and back of the substrate (gate) by thermal evaporation using shadow masks. Linear current versus voltage characteristics between drain and source confirms the Ohmic behavior of the electrodes, while the leakage current between the gate and source was less than 10 nA. The photoexcitation experiments were carried out in a closed cycle helium optical cryostat where the samples were exposed to the broadband radiation of a xenon lamp, whose spectrum contains ≃3.5% of UV radiation, and two single wavelength (441 and 325 nm) lines of a He-Cd laser through a quartz window.

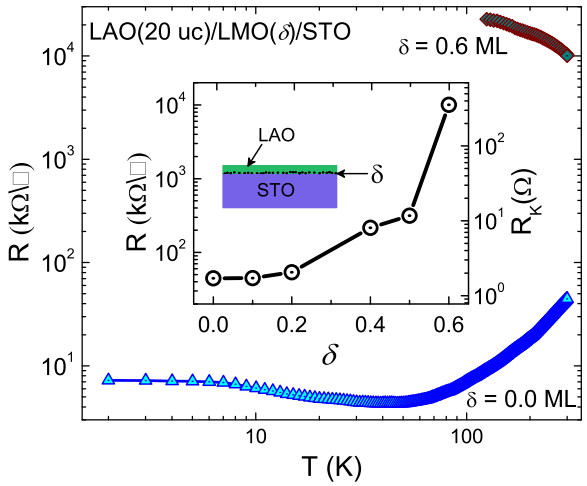

FIG. 1. (Color online) The temperature dependence of the sheet resistance ($R_\square$) for the samples with and without $LaMnO_3$ ($\delta = 0$ and 0.6 ML) at the $LaAlO_3/SrTiO_3$ interface. The $LaAlO_3/SrTiO_3$ sample shows a metallic behavior as the temperature is lowered to ≃30 K followed by an upturn, while the sample with 0.6 ML $LaMnO_3$ at the interface shows insulating behavior [40]. The resistance goes beyond the measurement limit below ≃120 K. The inset shows the variation of resistance at 300 K with the $LaMnO_3$ layer thickness in two different units, with the left axis representing it in units of kΩ while other axis is represented in the units of quantum resistance $R_k = h/e^2$, where h and e are the Planck's constant and electronic charge.

III. RESULTS

A. Electrical resistivity

The temperature dependence of the sheet resistance ($R_\square$) of the $LaAlO_3/SrTiO_3$ and that of the δ-$LaMnO_3$ doped samples are shown in Fig. 1. Consistent with the previous reports, a 20 unit cell thick $LaAlO_3$ film on TiO_2-terminated $SrTiO_3$ substrate showed metallic characteristics [16,17,40]. However, on embedding the $LaMnO_3$ sub-monolayer at the interface, we observe a systematic transition to insulating state. We have also noticed that the critical thickness of the $LaAlO_3$ overlayer required to induce 2DEG in δ-$LaMnO_3$ doped heterostructures is proportional to the sub-monolayer thickness of the δ-$LaMnO_3$ [40]. This study also revealed that ≃0.6 uc thick $LaMnO_3$ drives the interface to the insulating state when the $LaAlO_3$ overlayer thickness was of 20 uc. We note that the critical thickness of $LaMnO_3$ to make the interface insulating is much smaller when the $LaAlO_3$ layer is only 10 uc. The plot of $R_\square(T)$ for δ-doped $LaMnO_3$ with sub-monolayer thickness is shown in Fig. 1 along with $R_\square(T)$ of undoped $LaAlO_3/SrTiO_3$.

B. Photoresponse

Figure 2(a) shows the time evolution of resistance of three samples with $\delta \simeq 0,0.2$, and 0.5 ML during the period when sample was exposed to the light and then allowed to recover in dark at 20 K. To better understand the recovery process,

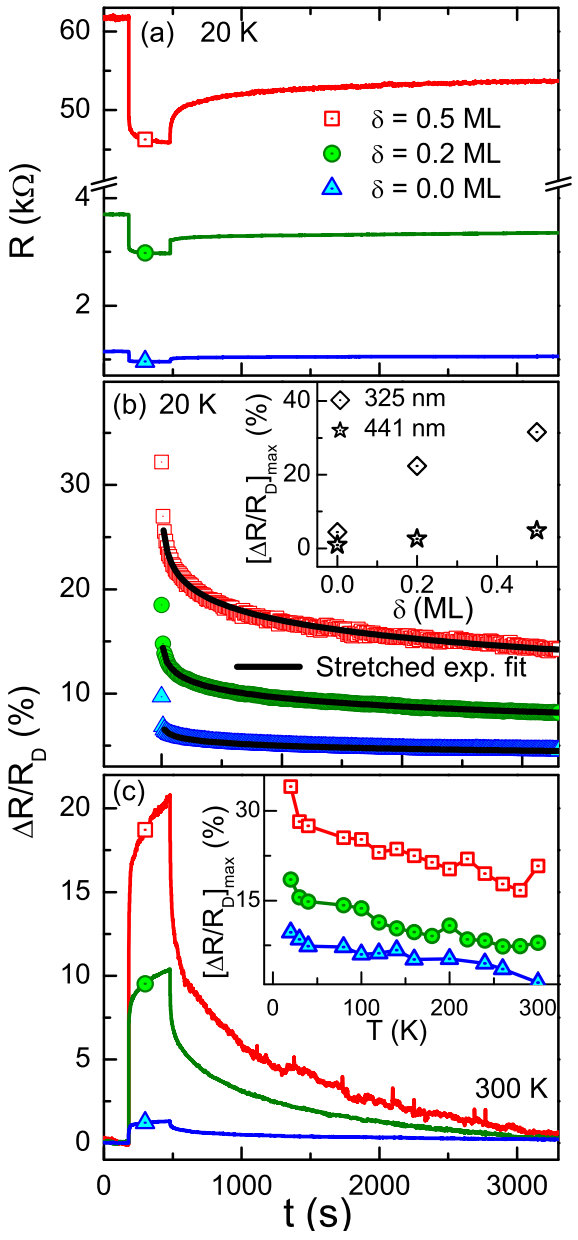

FIG. 2. (Color online) (a) The change in the channel resistance at 20 K as a function δ-layer thickness. The main panels (b) and (c) respectively show the relaxation of the normalized resistance for different δ doping at 20 and 300 K after switching off the illumination from a halogen lamp. The recovery dynamics follow a stretched exponential behavior which is represented as solid lines in (b). The inset of (b) shows the relative change in the resistance at 300 K upon radiating the samples with 325 and 441 nm lines of a He-Cd laser. A comparison of the photoresponse as a function of temperature for different samples is made in inset (c). The 0.5 monolayer $LaMnO_3$ shows a threefold increase in the photoresponse in comparison with the $\delta = 0$ sample.

TABLE I. A comparison of relative change in the resistance using different sources of radiation.

	$\delta = 0$	$\delta = 0.2$	$\delta = 0.5$
$(\Delta R/R_D)_{325\,\mathrm{nm}}$	0.0446	0.2236	0.3156
$(\Delta R/R_D)_{441\,\mathrm{nm}}$	0.0094	0.0258	0.0481
$(\Delta R/R_D)_{\mathrm{broadband}}$	0.0187	0.1079	0.2089

we have defined a normalized resistance $\Delta R/R_D$, where $\Delta R = R(t) - R_D$ with $R(t)$ being the resistance at time t and R_D the resistance in dark. The details of these measurement have been described in an earlier report [17]. Figures 2(b) and 2(c) reveal that the relative change in the resistance on photoexposure increases with δ-$LaMnO_3$ layer thickness, while the recovery process slows down. It is important to point out here that the most change in the resistance on photoexposure is triggered by the ultraviolet (UV) component of the quartz halogen lamp radiation. This fact is further established when we expose the sample to monochromatic radiations ($\lambda = 325$ and 441 nm) of the He-Cd laser. These results are shown in the inset of Fig. 2(b), from which we find that relative change in the resistance of all heterostructures under consideration is significantly suppressed for 441 nm radiation, in comparison to that observed under the 325 nm radiation. In Table I, we list the values of $\Delta R/R_D$ for all three samples achieved under 325 nm, 441 nm, and xenon lamp radiation. The comparative study as highlighted in Table I shows that the overall photoresponse increases with increasing δ doping of $LaMnO_3$ at the interface. Also, our data suggest that the threshold wavelength to induce photoconductivity in these heterostructures shifts towards higher wavelengths with δ doping. This effect has been qualitatively understood by means of band structure calculations, which is discussed in the next section.

In Fig. 2(c) we also show the $\Delta R/R_D$ data taken at 300 K and the temperature dependence of maximum $\Delta R/R_D$ (just after closing the shutter). The response decreases monotonically with increasing temperature and it is higher in δ-doped samples. However, before we discuss the decay of the PC state, it is worthwhile to compare the photoresponse of single-layer LMO grown on STO and a bare STO substrate subjected to growth conditions similar to that of LAO/LMO(δ)/STO heterostructures. The data shown in Fig. 3 were taken for the same separation between the drain and source electrodes as used in LAO/LMO(δ)/STO. The resistance of the sample in dark is >200 GΩ. Photoexposure brings it down to $\sim$130 GΩ. This percentage change in $\Delta R/R$ is nearly $\sim$40%. However, the overall six orders of magnitude higher resistance of the substrate will not change the PC properties of LAO/STO heterostructures. In the inset of Fig. 3 we show the recovery process of a bare STO sample which was kept at the growth temperatures for a slightly longer time, resulting in an overall lower resistance [15]. We note that the recovery process in bare STO is much faster than in the LAO/LMO(δ)/STO system [Fig. 2(c)].

In general, the recovery to the resistive state on shutting off the light is well described by a stretched exponential of the form $R \propto \exp[-(\frac{t}{\tau})^{\beta}]$ with $0 \leqslant \beta \leqslant 1$, and, τ being

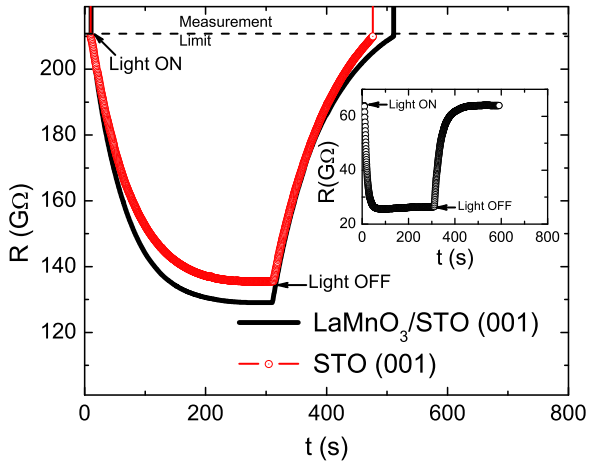

FIG. 3. (Color online) Main panel shows the photoconductivity behavior of a bare TiO_2-terminated STO and a LMO (1 uc)/STO. The sample resistance becomes measurable only after ∼10 s of light exposure. Inset is adapted from Ref. [15]. A complete recovery is seen here for a bare STO substrate. The recovery dynamics of bare STO also follow a stretched exponential behavior and extracted time constant (τ) is nearly ∼27 sec. A much shorter recovery time compared to data in Fig. 2 is noteworthy.

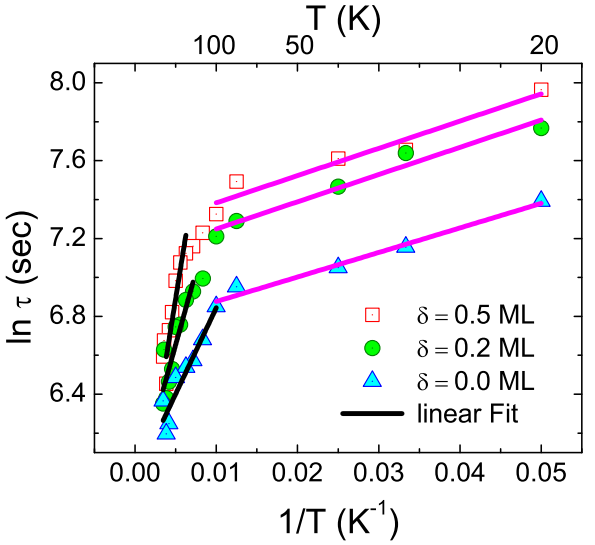

FIG. 4. (Color online) Comparison of the relaxation time constant (τ) of three system as indicated by the legends. The solid curves are the fits to the Arrhenius equation. The relaxation time constant scales in proportion with increasing $LaMnO_3$ sub-monolayer thickness. For system corresponding to 0.5 ML thick $LaMnO_3$, the relaxation time constant was estimated to be higher.

the relaxation time constant. A fit [shown by the solid lines in Fig. 2(b)] yields τ varying from 1700 to 3000 seconds as the thickness of the δ layer is increased to 0.5 uc. Correspondingly, the exponent β goes from 0.2 to 0.8. It is important to point out here that the recovery process in bare STO (Fig. 3) is much faster ($\tau_{STO} \sim 27$ sec) as compared to that seen in LAO/LMO(δ)/STO. This alludes towards some role of interface potentials in releasing the photogenerated carriers. Further, the recovery dynamics depend strongly on temperature. In order to understand the recovery process and the mechanisms involved, we fit the data to the Arrhenius equation given as $\tau = \tau_0 \exp(-\frac{\Delta U}{k_B T})$, where ΔU and k_B are the activation energy for detrapping the photogenerated carriers and Boltzmann constant, respectively. The plots of $\ln(\tau)$ against $(\frac{1}{T})$ are shown in Fig. 4. Clearly, two distinct temperature regions of activation can be seen in the Arrhenius plot. At low temperatures $T < 100$ K, the calculated value of ΔU is in the range 1–2 meV, for all samples. However, at higher temperatures, the ΔU for 0.5 uc thick $LaMnO_3$ is estimated as ≃22 meV, which is almost three times higher in comparison to the activation energy of the $LaAlO_3/SrTiO_3$ system (≃8 meV).

It is well known that the dielectric function of STO grows precipitously below the antiferro distortive cubic to tetragonal transition near ∼105 K [41]. Under these conditions the Bohr radius of the Ti d^1 electron near the oxygen vacancy is expected to be much larger than the lattice constant of STO. Such loosely bounded electrons are likely to be trapped and detrapped easily.

The electrical conductivity of these structures undergoes strong modulation when a gate field is applied. It has been shown earlier that the electrostatic and photon fields act on two different sets of charge carriers [17]. While the recovery time from the photoilluminated state stretches over several hours, the system was found to recover to the unperturbed normal state within microseconds after switching off the gate field. Hence, the role of the δ layer in influencing the migration of these two sets of carriers needs to be examined. We have studied the influence of electric field perturbation on the photoinduced relaxation processes of the δ-doped $LaMnO_3$ interfaces in comparison with that of the pure $LaAlO_3/SrTiO_3$ system.

In Fig. 5 we illustrate our measurement scheme to study the effects of a gate electric field on the recovery process. At point A of the plot in Fig. 5 the sample is exposed to light, which

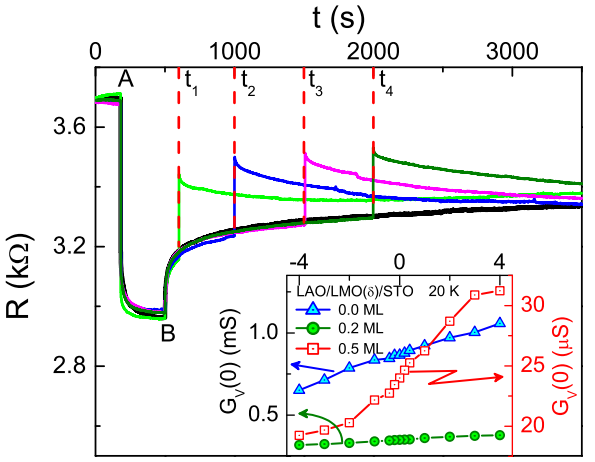

FIG. 5. (Color online) Main panel shows the effect of electric field in the PPC recovery state for $\delta = 0.2$ ML sample at 20 K. Points A and B in the figure show the time at which the illumination is turned ON and OFF, respectively. This photoinduced recovery state is then subjected to the gate field (E_g) at times t1, t2, t3, and t4. Inset shows the zero bias conductance [$G_V(0)$] of all three samples in dark at 20 K in the range ±4 kV/cm.

triggers a sharp drop in resistance followed by saturation. At point B the illumination is turned off and the recovery dynamics thereafter is examined by applying a gate field (E_g) of -2 kV/cm after a certain time gap, which has been changed from t_1 to t_4 in four sets of exposure-recovery experiments. We find that the resistance changes spontaneously on gating. While positive E_g enhances the channel conductivity, negative E_g tend to reduce it. For better understanding of the effect of gate field alone, we have measured source to drain *I-V* characteristic of these samples under different gate fields. The slope of these linear curves at the origin gives the zero-bias conductance $G_V(0)$ which is plotted in the inset of Fig. 5. We observe an order in magnitude decrease in the $G_V(0)$, in the $\delta = 0.5$ ML sample.

C. Electronic structure

The threshold energy required to impart photoconductivity in $LaAlO_3/SrTiO_3$ corresponds to that of near-ultraviolet wavelength. Numerical calculations based on density functional theory are consistent with this picture [17]. The optical transitions are associated with those states which are in the range ± 2 eV above and below the Fermi energy, thereby providing the estimate of photoconducting threshold wavelength as <500 nm.

However, the photoresponse of the δ-doped $LaAlO_3/SrTiO_3$ heterostructures shows subtle signatures of the photoresponse threshold shifting to lower photon energy, which suggests a modification in the band structure caused by the Mn ions in the vicinity of the interface. In Fig. 6, we show the band structure of the δ-doped $LaAlO_3/SrTiO_3$. A fully relaxed supercell of $2\times2\times9$ dimension with 4.5 unit cells of $SrTiO_3$ as substrate with TiO_2 termination is modeled in the present study. The δ doping with 0.5 ML thick $LaMnO_3$ is modeled by Mn-Al chemical disorder near the interface. The Brillouin zone integration was carried out on an $11\times11\times2$ k-space grid with the WIEN2K [42] parameters $RK_{\max}$ and $G_{\max}$ to be as 7 and 24, respectively. The numerical details of the structure optimization, self-consistent total energy, and electronic structure are similar to those described in Ref. [17]. Both in the local density approximation (LDA) and generalized gradient approximation (GGA), Mn ions modeled at the interface of the $LaAlO_3/SrTiO_3$ system yield a metallic state, with relatively high density of states, with the prominent states being the Mn $3d$ states. It is well known that such spurious states at the Fermi energy are due consequence of the missing Coulomb correlation term in the Hamiltonian. In the present case, the Coulomb correlation effects (U_{eff}) of the Mn $3d$ electrons are taken into consideration by the LDA+U_{eff} Hamiltonian, with $U_{\text{eff}} = 8$ eV.

Before we discuss the band structure of the δ-doped $LaMnO_3$, recall from Fig. 9 of Ref. [17] that the calculated optical conductivity of the $LaAlO_3/SrTiO_3$ heterostructure matches well with that of the experiments. The consistency indicates the reliability of the band structure generated in the density functional theoretical formalism. The upper valence band of the $LaAlO_3/SrTiO_3$ system is primarily composed of O $2p$ states of the AlO_2 layers of the $LaAlO_3$ film. Electronic states, $\simeq2$ eV below the Fermi energy, are the O $2p$ states of the TiO_2 layers of the substrate. On the other hand, the states

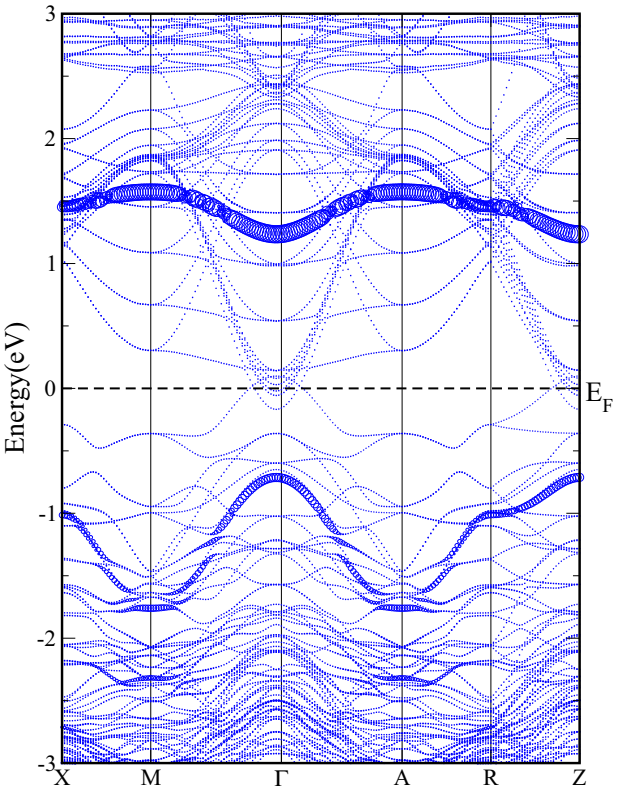

FIG. 6. (Color online) Fat band representation of the Mn $3d$ majority states (circle) of the δ-doped $LaMnO_3$ in $LaAlO_3/SrTiO_3$ heterostructures, calculated using the LDA+U method, with $U = 8$ eV. The conduction band around $E \simeq 1.5$ eV is derived from the Mn $3d_{z^2}$ spin-up states, while that in the valence band in the range $1.7 < E$ (eV) < 0.5 corresponds to the Mn $3d_{xy}$ spin-up states.

above Fermi energy are primarily composed of Ti $3d$ orbitals. At energies $\geqslant2$ eV above Fermi energy, one finds a bunching of Ti $3d$ bands of primarily the e_g character. These states are relatively localized over a very narrow energy interval. Thus, photoconductivity in $LaAlO_3/SrTiO_3$ heterostructures results from the interband transitions between Ti-derived e_g bands and that of the O $2p$–Ti t_{2g} amalgamation at the Fermi energy.

In the case of δ-doped $LaAlO_3/SrTiO_3$ with $LaMnO_3$ monolayers, the band structure as shown in Fig. 6 shows localized Mn $3d_{z^2}$ states (e_g states) positioned $\simeq1.5$ eV above the Fermi energy. The corresponding Mn $3d_{xy}$ states (t_{2g}) in the valence band are relatively more dispersed over a wider energy range. Thus, it is evident that the positioning of the Mn e_g states within the photoconducting gap leads to a decrease in the photoexcitation energy, and therefore is expected to increase the overall photoresponse. Thus, for small wavelength-induced excitations one finds the transition to occur between the states that lie between ±2eV of the Fermi energy, while the small photogeneration of carriers at the 441 nm is associated with the Ti $3d_{xy}$ states near the Fermi energy and the Mn e_g bands which are relatively 1.5 eV above the Fermi energy.

The computed band structure also qualitatively explains the relatively slow relaxation of the photogenerated carriers to the normal state in the δ-doped systems with that of the pure $LaAlO_3/SrTiO_3$. The energy-time relation of the uncertainty

principle suggests that the life-time of photogenerated carriers in a given band would be inversely proportional to the energy bandwidth. Along these perspectives, finding that the Mn e_g bands which are highly localized and positioned at 1.5 eV above the Fermi energy would serve as localized traps for the photo-induced charge carriers, thereby increasing the relaxation time in δ-doped systems in comparison with the parent system.

IV. DISCUSSION

For abrupt interfaces of oxide heterostructures, the polar catastrophe model is quite robust to account for the origin of 2DEG. The model asserts band-bending effects via electronic reconstruction due to the in-built electric field at the interface of the polar ($LaAlO_3$)–nonpolar ($SrTiO_3$) materials. PPC in these systems can therefore be related to the model proposed by Queisser and Theodorou (QT), where its emergence is associated with the macroscopic potential barriers induced by the band-bending effects [43]. Such potential barriers lead to the PPC effect by spatial separation of the photogenerated electrons and holes. With one type of carrier being trapped, the other remains free and causes excess conductivity [44]. The model can be verified by studying the excitation-energy dependence of PPC. For this we used the two excitation energies afforded from He-Cd laser, which gives one of the excitation energies (2.8 eV) less while the other one larger (3.8 eV) than the band gap energy of $SrTiO_3$. The results are displayed in Table I and the inset of Fig. 2(b). For pure $LaAlO_3/SrTiO_3$ heterostructures, we observed very small change in the resistance and also weak signature of PPC with the photoexcitation below the absorption edge, while for δ-doped samples a large PPC effect could be seen, which increases monotonically with the δ-layer thickness. These results infer that the PPC of the undoped sample has little contribution arising from spatial separation of the photogenerated carriers, primarily due to the band-bending effects, while in the case of δ-doped systems, this effect seems to be less prominent. The change in the resistance of δ-doped systems with lower excitation can be attributed to the finite absorption of incident illumination by in-gap states present in the $SrTiO_3$ band gap and reduce the possibility of the band-bending scenario. It has also been shown that the 2DEG confinement can be explained by the formation of metal-induced gap states in the band gap of $SrTiO_3$ rather than the band bending [32] and no measurable band bending is observed in $La_{1-x}Al_{1+x}O_3/SrTiO_3(001)$ heterojunctions [45]. Thus, the model based on the spatial separation of the photoexcited electrons and holes by a macroscopic potential barrier due to band bending looks less appropriate to account for the PPC here. However, if the band bending is due to the O vacancies, then the associated barrier would spatially separate the electrons that constitute the 2DEG. Although this can lead to some justification of the QT model to the observed PPC effects in the present heterostructured systems, the observed decay kinetics does not seem to support the model as a predominant process for inducing PPC. The above picture of band bending is further established by the analysis of the PPC decay dynamics as proposed in the QT model for artificially tailored heterostructures [43]. We tried to fit the decay to a logarithmic behavior of the form $\Delta R/R_D = a - b[\ln(1 + t/\tau)]$, where a and b are constants, with respect to time. We find that the logarithmic fit becomes poorer and deviates significantly from the measured data as the δ-layer thickness is increased. However, the undoped system still displays a better χ^2 tolerance to the fit and low residual values as compared to the δ-doped samples, which strengthens our argument.

Various other models have also been proposed to account for the PPC effects in solid state materials [43,46–50]. The earliest of all was associated with inhomogeneities in the samples, caused by bonding configurations or spatial variation in the chemical composition and/or in local charge densities. A much more advanced model was due to Theodorou and Symeonides [51], who proposed the role of defect clusters in the sample. Such defects may be inevitable and are generally introduced during the growth itself. On preliminary grounds, the defect-cluster model may look appropriate to account for PPC in these heterostructures, as the synthesis technique employed in depositing δ-doped $LaAlO_3$ films on $SrTiO_3$ substrates are by means of the laser ablation. This highly energetic deposition process could result in clusterization of the Mn and Al ions forming a disordered $LaAl_{1-x}Mn_xO_3$ monolayer. In cases where the local inhomogeneities lead to a density of the defects which is larger than the carrier density, a macroscopic potential barrier may be formed. Such defect clusters may host traps, and upon electron capture would become charged. In turn, this would induce a charge of opposite polarity around the cluster, thus spatially separating the electron-hole pairs, impeding their recombination and resulting in PPC [51,52]. However, the defect-cluster model predicts larger PPC in proportion to the thickness of the conducting layer. The latter, however, is in contrast with our observation in δ-doped $LaMnO_3$ in the $LaAlO_3/SrTiO_3$ interface. We find that as the δ-doped sub-monolayer thickness is increased (larger Al/Mn disorder), the 2DEG conductivity decreases, but with an enhancement in the PPC. Thus, the defect-cluster model also seems less appropriate to account for the larger PPC seen in the δ-doped $LaMnO_3$ in the samples.

A relevant model that appears to describe the PPC in the present case is based on potential fluctuations in the material [47,53–57]. Here the spatial separation between photoexcited charge carriers by random local-potential fluctuations induced by compositional variations is held responsible for PPC [47]. Within the framework of the polar catastrophe model, the origin of 2DEG is due to electronic reconstruction of the Ti ions at the interface. Thus, the 2DEG wave function would be thought as a composition of Ti^{3+} and Ti^{4+} states. Moreover, the Mn ions in the monolayer would also exhibit multiple valence states. Certainly therefore, an energy barrier emanating from such a charge fluctuation would also act as a source of potential fluctuations. Besides, there is also a likelihood of chemical disorder due to random distribution of Al and Mn ions in the δ-doped layer. Therefore, both chemical and valence state disorder can induce an uneven potential landscape at the interface of $LaAlO_3/SrTiO_3$ with δ doping of the interface. However, this model predicts PPC to be observed at high temperatures, with a well-defined transition temperature, which is in contrast with our observations, where enhanced PPC in seen at lower temperatures. But, we note that the decay

kinetics predicted by the random potential fluctuation model is similar to that of a stretched exponential function.

The lattice relaxation model [50,58,59] is one of the most widely accepted descriptions for the PPC effects in semiconductor heterostructures. The model stipulates photoexcitation of carriers from defect-induced deep-level traps. A barrier is created by lattice relaxation thereby preventing the recapture of mobile carriers. The source of the lattice relaxation could be ionic mismatch and/or vacancies. However, in the present context, mismatch in the lattice constants and/or that in the constituents' ionic radii does not seems to be relevant. Therefore, the structural relaxation would be mainly due to oxygen vacancies, and hence these defects render a negative-U center. At low temperatures, thermal energy is not sufficient enough to overcome the barrier, and thus the photogenerated carriers remain in these shallow states, resulting in PPC. The PPC buildup and decay kinetics, in general, fit to a stretched exponential curve, which is similar to our observations for the oxide heterostructures [16,17]. Due to the inherent propensity of $LaMnO_3$ to attract oxygen, its presence in the vicinity of the interface can induce more vacancies in the substrate leading to a nonequilibrium chemical configuration. Thus, while the photoionization of oxygen specific defects in the quantum well region appears to be the dominant mechanism for PPC in oxide heterostructures, one cannot rule out the contribution of the spatially separated charges across the interface facilitated by the factors that have been mentioned above.

Moreover, as both Mn and Al occupy the substitutional body-centered site of the perovskite structure, the role of Mn ions on the lattice can also be partly inferred from the PPC data. It has been argued in the case of III-V and II-IV semiconductor heterostructures and also in oxide heterostructures that the 2DEG at the interface is derived out of lattice strain. Within the realms of alloy theory, the solubility of Mn ions in $LaAlO_3$ matrix infers a lowering of lattice strain. In general, reduction of strain decreases the activation energy with Mn at. % in the monolayer, which, however, is in contradiction with our observation. Thus, the increase in activation energy with δ doping at the interface may be attributed to the enhanced electron-electron interaction between the electrons in the trap and the unpaired electrons of the Mn ion. Such an event leads to a narrowing of the optical trap potential, which would narrow with increasing Mn at. % at the interface, leading to a higher repulsive barrier for the electrons to return to the oxygen mediated defect centers, after photoionization. However, we note that there does not exist to the best of our knowledge a scheme to estimate the strength of Coulomb scattering from the presence of the deep traps in the quantum well and its effect on transport properties. However, it is reported that in ZnSe/(Zn,Cd,Mn)Se heterostructured systems, the 2DEG exhibits a strong PPC that becomes more pronounced when the Mn^{2+} concentration is increased [60]. The enhanced PPC in this system is also accompanied by a decrease in sample mobility, suggesting a connection between the deep traps introduced by the magnetic Mn ions and enhanced Coulomb scattering.

V. CONCLUSION

In summary, we have investigated the effect of δ-doping on the photoresponse of $LaAlO_3/SrTiO_3$ interfaces. The photoresponse of the pure $LaAlO_3/SrTiO_3$ heterostructure is found to be sensitive to near-ultraviolet radiation which shifts towards the lower photon energy upon doping the interface with $LaMnO_3$. The doped samples show relatively large photoresponse and time constant of recovery in comparison to the undoped sample. Based on theoretical calculations, we establish that the slow relaxation arises due to localized Mn e_g states ($3d_{z^2}$) which are situated $\sim$1.5 eV above the Fermi level. The positioning of these Mn $3d$ e_g bands within the photoconducting gap shifts the photoresponse threshold to higher photon wavelengths with increasing δ doping in the heterostructures. We also have made an attempt to understand the decay dynamics of the photoconducting state. Our experimental findings demonstrate that the defect-cluster and random fluctuation models are less appropriate to describe the large photoresponse and high values of activation energies for the recovery seen in δ-doped samples. On other hand, the lattice relaxation model is found to be in better agreement. Moreover, our arguments also suggest that the increase in the activation energy could be attributed to the strong electron-electron interaction of the Mn ions in the δ-doped monolayer at the interface. A dramatic drop in activation energy for recovery below 100 K appears to be related to the large gain in the dielectric function of $SrTiO_3$.

ACKNOWLEDGMENTS

The authors gratefully acknowledge discussions with S. Auluck. A.R. would like to acknowledge the Council of Scientific and Industrial Research (CSIR), India, and Indian Institute of Technology Kanpur for financial support. R.C.B. acknowledges financial support from a J. C. Bose National Fellowship of the Department of Science and Technology, Government of India.

[1] A. Ohtomo, A. D. Muller, J. L. Grazul, and H. Y. Hwang, Nature (London) **419**, 378 (2002).

[2] A. Ohtomo and H. Y. Hwang, Nature (London) **427**, 423 (2004).

[3] A. Ohtomo and H. Y. Hwang, Nature (London) **441**, 120 (2006).

[4] S. Thiel, G. Hammer, A. Schmehl, C. W. Schneider, and J. Mannhart, Science **313**, 1942 (2006).

[5] A. D. Caviglia, S. Gariglio, C. Cancellieri, B. Sacépé, A. Fête, N. Reyren, M. Gabay, A. F. Morpurgo, and J.-M. Triscone, Phys. Rev. Lett. **105**, 236802 (2010).

[6] M. Huijben, G. Rijnders, D. H. A. Blank, S. Bals, S. Van Aert, J. Verbeeck, G. Van Tendeloo, A. Brinkman, and H. Hilgenkamp, Nat. Mater. **5**, 556 (2006).

[7] S. Okamoto and A. J. Millis, Nature (London) **428**, 630 (2004).

[8] W. Siemons, G. Koster, H. Yamamoto, W. A. Harrison, G. Lucovsky, T. H. Geballe, D. H. A. Blank, and M. R. Beasley, Phys. Rev. Lett. **98**, 196802 (2007).

[9] A. Kalabukhov, R. Gunnarsson, J. Börjesson, E. Olsson, T. Claeson, and D. Winkler, Phys. Rev. B **75**, 121404 (2007).

[10] G. Herranz, M. Basleticacute, M. Bibes *et al*., Phys. Rev. Lett. **98**, 216803 (2007).

[11] Y. Tokura, Y. Taguchi, Y. Okada, Y. Fujishima, T. Arima, K. Kumagai, and Y. Iye, Phys. Rev. Lett. **70**, 2126 (1993).

[12] J. J. Pulikkotil, S. Auluck, P. Kumar, A. Dogra, and R. C. Budhani, Appl. Phys. Lett. **99**, 081915 (2011).

[13] M. Huijben, A. Brinkman, G. Koster, G. Rijnders, H. Hilgenkamp, and D. H. A. Blank, Adv. Mater. **21**, 1665 (2009).

[14] G. Herranz, M. Basletić, O. Copie, M. Bibes, A. N. Khodan, C. Carrétéro, E. Tafra, E. Jacquet, K. Bouzehouane, A. Hamzić, and A. Barthélémy, Appl. Phys. Lett. **94**, 012113 (2009).

[15] A. Rastogi, A. K. Kushwaha, T. Shiyani, A. Gangawar, and R. C. Budhani, Adv. Mater. **22**, 4448 (2010).

[16] A. Rastogi and R. C. Budhani, Opt. Lett. **37**, 317 (2012).

[17] A. Rastogi, J. J. Pulikkotil, S. Auluck, Z. Hossain, and R. C. Budhani, Phys. Rev. B **86**, 075127 (2012).

[18] N. Sakai, H. Fjellvåg, and B. C. Hauback, J. Solid State Chem. **121**, 202 (1996).

[19] P. Schiffer, A. P. Ramirez, W. Bao, and S.-W. Cheong, Phys. Rev. Lett. **75**, 3336 (1995).

[20] J.-H. Park, E. Vescovo, H.-J. Kim, C. Kwon, R. Ramesh, and T. Venkatesan, Nature (London) **392**, 794 (1998).

[21] S. A. Chambers, L. Qiao, T. C. Droubay, T. C. Kaspar, B. W. Arey, and P. V. Sushko, Phys. Rev. Lett. **107**, 206802 (2011).

[22] J. Garcia-Barriocanal, F. Y. Bruno, A. Rivera-Calzada, Z. Sefrioui, N. M. Nemes, M. Garcia-Hernández, J. Rubio-Zuazo, G. R. Castro, M. Varela, S. J. Pennycook, C. Leon, and J. Santamaria, Adv. Mater. **22**, 627 (2010).

[23] N. Nakagawa, H. Y. Hwang, and D. A. Muller, Nat. Mater. **5**, 204 (2006).

[24] M. Stengel and D. Vanderbilt, Phys. Rev. B **80**, 241103 (2009).

[25] R. Pentcheva and W. E. Pickett, J. Phys. Condens. Matter **22**, 043001 (2010).

[26] H. Chen, A. M. Kolpak, and S. Ismail-Beigi, Phys. Rev. B **79**, 161402 (2009).

[27] W.-J. Son, E. Cho, B. Lee, J. Lee, and S. Han, Phys. Rev. B **79**, 245411 (2009).

[28] G. S. Bhalla, C. Bell, J. Ravichandran, W. Siemons, Y. Hikita, S. Salahuddin, A. F. Hebard, H. Y. Hwang, and R. Ramesh, Nat. Phys. **7**, 80 (2011).

[29] Y. Segal, J. H. Ngai, J. W. Reiner, F. J. Walker, and C. H. Ahn, Phys. Rev. B **80**, 241107 (2009).

[30] S. A. Chambers, M. H. Engelhard, V. Shutthanandan, Z. Zhu, T. C. Droubay, L. Qiao, P. V. Sushko, T. Feng, H. D. Lee, T. Gustafsson, E. Garfunkel, A. B. Shah, J.-M. Zuo, and Q. M. Ramasse, Surf. Sci. Rep. **65**, 317 (2010).

[31] K. Yoshimatsu, R. Yasuhara, H. Kumigashira, and M. Oshima, Phys. Rev. Lett. **101**, 026802 (2008).

[32] K. Janicka, J. P. Velev, and E. Y. Tsymbal, Phys. Rev. Lett. **102**, 106803 (2009).

[33] D. C. Tsui, H. L. Stormer, and A. C. Gossard, Phys. Rev. Lett. **48**, 1559 (1982).

[34] A. D. Caviglia, S. Gariglio, N. Reyren, D. Jaccard, T. Schneider, M. Gabay, S. Thiel, G. Hammerl, J. Mannhart, and J.-M. Triscone, Nature (London) **456**, 624 (2008).

[35] T. Ishikawa, M. Itoh, M. Kurita, H. Shimoda, M. Takesada, T. Yagi, and S. Koshihara, Ferroelectrics **298**, 141 (2004).

[36] O. Tikhomirov, H. Jiang, and J. Levy, Phys. Rev. Lett. **89**, 147601 (2002).

[37] T. Feng, Phys. Rev. B **25**, 627 (1982).

[38] E. Arslan, S. Bütün, S. B. Lisesivdin, M. Kasap, S. Ozcelik, and E. Ozbay, J. Appl. Phys. **103**, 103701 (2008).

[39] H. L. Störmer, R. Dingle, A. C. Gossard, W. Wiegmann, and M. D. Sturge, Solid State Commun. **29**, 705 (1979).

[40] A. Rastogi, S. Tiwari, J. J. Pulikkotil, Z. Hossain, D. Kumar, and R. C. Budhani, arXiv:1306.1494.

[41] Y. Kozuka, Y. Hikita, T. Susaki, and H. Y. Hwang, Phys. Rev. B **76**, 085129 (2007).

[42] P. Blaha, K. Schwarz, G. Madsen, D. Kvasicka, and J. Luitz, computer code WIEN2K, Technical University of Vienna, 2001.

[43] H. J. Queisser and D. E. Theodorou, Phys. Rev. B **33**, 4027 (1986).

[44] Y. C. Lee, J. L. Shen, K. W. Chen, W. Z. Lee, and S. Y. Hu, J. Appl. Phys. **99**, 063706 (2006).

[45] L. Qiao, T. C. Droubay, T. C. Kaspar, P. V. Sushko, and S. A. Chambers, Surf. Sci. **605**, 1381 (2011).

[46] P. M. Mooney, N. S. Caswell, and S. L. Wright, J. Appl. Phys. **62**, 4786 (1987).

[47] H. X. Jiang and J. Y. Lin, Phys. Rev. B **40**, 10025 (1989).

[48] W. Iseler, J. A. Kafalas, and A. J. Strauss, Solid State Commun. **10**, 619 (1972).

[49] E. F. Schubert and K. Ploog, Phys. Rev. B **29**, 4562 (1984).

[50] D. V. Lang and R. A. Logan, Phys. Rev. Lett. **39**, 635 (1977).

[51] D. E. Theodorou and C. I. Symeonidis, Phys. Rev. B **37**, 10854 (1988).

[52] D. E. Theodorou and H. J. Queisser, Appl. Phys. **23**, 121 (1980).

[53] S. Permogorov, A. Reznitskii, S. Verbin, and V. Lysenko, Solid State Commun. **47**, 5 (1983).

[54] E. Cohen and M. D. Sturge, Phys. Rev. B **25**, 3828 (1982).

[55] H. X. Jiang, L. Q. Zu, and J. Y. Lin, Phys. Rev. B **42**, 7284 (1990).

[56] H. X. Jiang and J. Y. Lin, Phys. Rev. Lett. **64**, 2547 (1990).

[57] J. Y. Lin, A. Dissanayake, and H. X. Jiang, Phys. Rev. B **46**, 3810 (1992).

[58] D. V. Lang, R. A. Logan, and M. Jaros, Phys. Rev. B **19**, 1015 (1979).

[59] B. L. Zhou, K. Ploog, E. Gmelin, X. Q. Zheng, and M. Schulz, Appl. Phys. A **28**, 223 (1982).

[60] O. Ray, I. P. Smorchkova, and N. Samarth, Phys. Rev. B **59**, 9810 (1999).